Desalination and Water Treatment
www.deswater.com

doi: 10.5004/dwt.2023.29351

287 (2023) 124–138
March

Degradation of enrofloxacin in water by Fe_3O_4@TiO_2 magnetic photocatalyst: optimization of environmental factors

Vo Thi Thanh Thuy[a,b], Dao Nhat Tan[c], Nguyen Le Phuc Khai[c], Nguyen Thi Thuy[b,d], Nguyen Thi Cam Tien[a,b], Lam Pham Thanh Hien[a,b], Dang Van Thanh[e], Nguyen Nhat Huy[a,b,*]

[a]*Faculty of Environment and Natural Resources, Ho Chi Minh City University of Technology (HCMUT), 268 Ly Thuong Kiet St., Dist. 10, Ho Chi Minh City, Vietnam, emails: nnhuy@hcmut.edu.vn (N.N. Huy), vtthuy@hcmut.edu.vn (V.T.T. Thuy), tien.nguyen.ktmt@gmail.com (N.T.C. Tien), lamhien87@hcmut.edu.vn (L.P.T. Hien)*
[b]*Vietnam National University Ho Chi Minh City, Linh Trung Ward, Thu Duc City, Ho Chi Minh City, Vietnam, email: ntthuy@hcmiu.edu.vn (N.T. Thuy)*
[c]*Faculty of Chemical and Food Technology, Ho Chi Minh City University of Technology and Education, 01 Vo Van Ngan Street, Thu Duc City, Ho Chi Minh City, Vietnam, emails: tandaohse@gmail.com (D.N. Tan), khai.nguyenlephuc@gmail.com (N.L.P. Khai)*
[d]*School of Chemical and Environmental Engineering, International University, Quarter 6, Linh Trung Ward, Thu Duc City, Ho Chi Minh City, Vietnam*
[e]*Faculty of Basic Sciences, TNU-University of Medicine and Pharmacy, 284 Luong Ngoc Quyen Rd., Thai Nguyen City, Viet Nam, email: thanhdv@tnmc.edu.vn (D.V. Thanh)*

Received 5 March 2022; Accepted 5 February 2023

ABSTRACT

In recent years, water pollution caused by antibiotics, contaminants of emerging concern, is a hot issue that attracts much attention. In this study, TiO_2 prepared by the sol–gel method was impregnated on a Fe_3O_4 ferromagnetic core to form a core-shell composite of Fe_3O_4@TiO_2 magnetic photocatalyst. The material properties were determined using scanning electron microscopy, energy-dispersive X-ray spectroscopy, vibrating sample magnetometry, X-ray diffraction, Raman, Fourier-transform infrared spectroscopy, Brunauer–Emmett–Teller, and UV-Visible diffuse reflectance spectroscopy techniques. The photocatalytic activity and recoverability of the Fe_3O_4@TiO_2 magnetic material were evaluated via its performance for enrofloxacin (ENR) degradation in water. The effects of various factors (e.g., pH, catalyst dosage, ENR concentration, and treatment time) on ENR degradation were investigated. Design-Expert software was then used for the experimental design and optimization of the ENR degradation. Results showed that the ENR degradation efficiency after 2.5 h was over 90% under UVA irradiation, at pH 7, catalyst dose of 0.972 g/L, and initial ENR concentration of 19.628 mg/L. After treatment, 62% of the material was recoverable by an external magnetic field, suggesting a potential solution for the treatment of antibiotics in water with high degradation efficiency and material recovery.

Keywords: Antibiotics; Magnetic photocatalyst; Fe_3O_4@TiO_2; Enrofloxacin

* Corresponding author.

1. Introduction

Antibiotics are emerging pollutants that occur in the natural environment from pharmaceutical industry waste, hospital wastewater, and human and animal excretion products. Centralized wastewater treatment systems, municipal wastewater treatment plants, and hospitals are also hotspots and sources of antibiotic residue emissions into the natural environment [1–3] because about 18%–66% of antibiotics are not completely removed using conventional wastewater treatment systems [4]. Therefore, it is necessary to study antibiotic treatment solutions to prevent unintended incidents. Enrofloxacin (ENR), an antibiotic belonging to the fluoroquinolones group with the structural formula of $C_{19}H_{22}FN_3O_3$, has a high bactericidal effect and a broad antibacterial spectrum that inhibits both gram-positive and gram-negative bacteria. ENR is commonly used to treat respiratory and intestinal infections in veterinary medicine [5]. ENR was detected in almost all areas of rivers, city canals, centralized wastewater treatment systems, and livestock/aquaculture wastewater around the world [6–9], especially in India [10,11] and China [12]. ENR concentration fluctuates around several tens of ppb in the aquatic environment [13] with ENR residues in pharmaceutical wastewater in India of 210–900 μg/L [10,11]. The sustainable and stable existence of ENR in the environment, especially its strong adsorption capacity into the soil, has contributed to its negative impact on ecosystems and humans even at low concentrations [14].

Several methods have been studied and applied in the treatment of antibiotic residues, including physico-chemical treatment, biological treatment, and advanced oxidation processes (AOPs). Accordingly, the biological method is unstable with the treatment efficiency varying from 50% to 98% and the physico-chemical method cannot completely deal with the production of secondary pollutants. AOPs are often considered the most suitable treatment technology for emerging pollutants with stable treatment efficiency and the ability to thoroughly decompose the pollutants into environmental-friendly compounds and even mineralized products. Among AOPs, photocatalysis provides high catalytic efficiency and simplicity in operation, which has been extensively studied for the removal of organic pollutants. Some commonly known photocatalyst materials are TiO_2, ZnO, WO_3, SnO_2, α-Fe_2O_3, and sulfide semiconductor compounds (e.g., ZnS, CdS, and WS_2). Previous studies have shown that photocatalysis with TiO_2 can effectively decompose hard-biodegradable substances in water such as pesticides, dyes, organics, and especially antibiotics [15–18]. The combination of Bi_2O_3 (*n*-type) and TiO_2 (*n*-type, sphere) catalyzed the complete degradation of total organic carbon and tetracycline at its characteristic peak (~ 350 nm) under visible light (λ > 420 nm) [15]. Giraldo et al. [16] used TiO_2 (Degussa P25) suspension to degrade the oxolinic acid at a concentration of 20 mg/L. The result showed that degradation efficiency was enhanced at low pH and catalyst dosage of 1 mg/L. The antibacterial activity, as well as antibiotic toxicity, decreased by 60% after 30 min of treatment under optimal conditions. The mechanisms of degradation of ciprofloxacin along with intermediate products during treatment with heterogeneous TiO_2 were proposed in the study of Hu et al. [17]. In addition, this report also summarized the remarkable progress in the degradation of ciprofloxacin by photocatalysis under visible light irradiation.

Besides many advantages, photocatalysis using TiO_2 also has certain disadvantages such as high recombination of photo-generated electrons and holes or the use the light of short wavelength ultraviolet (UV) range. Surface modification or doping TiO_2 with metal/non-metal can limit electron–hole recombination and shift the utilized range of light into the visible light region. The modifications with alkali metals (e.g., Na, K, Li), metals (e.g., Fe, Cr, Co, V, Cu, Nd, Ce, Zr, and Sn), and non-metals (e.g., B, C, N, F, S, Cl, and Br) help increase the photocatalytic activity of TiO_2 in the visible light region [19]. On the other hand, the main limitation of photocatalysis is the low recovery ability of the used material after water treatment. This can lead to the contamination of nanomaterials in the water environment, adversely affecting ecosystems and the life of organisms as well as humans. Centrifugation or filtration for separating nanomaterials after treatment is difficult to be applied in practice because of the high requirements of equipment, energy, and cost. Thus, the development of magnetic photocatalytic materials that can be easily recovered by a magnetic field is an interesting research field since it is energy-saving and simple to operate [20–22]. Furthermore, since the magnetic field can pass through some materials such as glass or plastic without any physical interaction with the material, it will not contaminate the water source. In addition, this separation is not sensitive to environmental factors such as pH, temperature, and ionic concentration of the solution, which does not affect the photocatalytic activity. Especially, magnetic photocatalysts based on ferromagnetic cores [23] such as superparamagnetic materials of Fe_3O_4-TiO_2 have a high saturation magnetization of 49 emu/g [24]. He et al. [25] prepared Fe_3O_4-TiO_2 by homogeneous precipitation method, which had high activity and no toxicity and can work with visible light. The TiO_2 layer thickness on the magnetic core also significantly affected the photocatalytic efficiency [26]. The composites with a TiO_2 layer thickness of 17 nm gave high activity and had an extended light absorption band (>600 nm). Therefore, there is a great opportunity for improving the recovery ability of the nanomaterial while keeping its photocatalytic activity via the core-shelf structure of Fe_3O_4-TiO_2. Besides, this structure is expected to enhance the efficiency of ENR photocatalysis by reducing the band gap energy compared to TiO_2, thereby improving light efficiency.

In this study, the combination of precipitation, sol–gel, and hydrothermal methods was applied to synthesize Fe_3O_4@TiO_2 magnetic photocatalyst. The photocatalytic activity of the material was evaluated via its ability for removing ENR in water. The effects of pH, photocatalyst dosage, initial ENR concentration, and treatment time on ENR degradation efficiency were investigated. The Design-Expert software was used to build multivariable equations to find suitable operating conditions for optimal treatment efficiency.

2. Materials and methods

2.1. Synthesis and characterization of materials

The chemicals used in this study were all analytical grade and bought from China. The water used in this study was

double-distilled and it was taken from a local machine in the laboratory.

A mixture of $FeCl_2$ and $FeCl_3$ in an alkaline solution was used to produce the Fe_3O_4 core, following a procedure reported in the literature [27] with some minor modifications. In a typical process, 1.99 g of $FeCl_2{\cdot}4H_2O$ and 5.40 g of $FeCl_3{\cdot}6H_2O$ (molar ratio of 1:2) were added into a flask containing 50 mL of water. The mixture was then stirred at 1,000 rpm, heated to 80°C, and slowly added with NaOH solution with the molar ratio $8OH^-$:$1Fe^{2+}$:$2Fe^{3+}$. After the color changed from orange to brown and finally to black, the mixture was continuously stirred at 80°C for 1 h to achieve the complete reaction. After that, the mixture was washed and filtered with water about 7–10 times, and finally dried at 105°C for 12 h to obtain the Fe_3O_4 powder.

Fe_3O_4@TiO_2 magnetic photocatalyst was then synthesized by sol–gel and hydrothermal methods [25]. The preparation procedure began with the preparation of S (40 mL ethanol and 40 mL *n*-propanol), S1 (20 mL of S solution, 0.76 mL of water, and 0.055 mL of 68% HNO_3 solution), and S2 (20 mL of S solution and 15 mL of titanium isopropoxide (TTIP)) solutions. At first, the S1 solution was stirred in a flask at 500 rpm for 30 min, which was then slowly added with the entire amount of the prepared S2 solution. This mixture was subsequently heated to 80°C and the stirring speed was adjusted to 750 rpm to obtain a gel. This gel was then transferred into an autoclave and hydrothermally treated at 150°C for 12 h. The gel after hydrothermal was mixed with the previously prepared Fe_3O_4 powder and shaken at 220 rpm for 45 min. After that, the mixture was filtered and dried at 105°C for 2 h to obtain the Fe_3O_4@TiO_2 material. In the case that Fe_3O_4 powder was not added to the solution after hydrothermal, the obtained material was TiO_2 powder with white color.

The morphological and elemental composition of the materials was determined by scanning electron microscopy (SEM) and energy-dispersive X-ray spectroscopy (EDX), respectively (JSM-IT200, JEOL, Japan). The crystal phase structure and magnetic properties were examined by X-ray diffraction (XRD, D2 PHASER, Bruker, Germany) and vibrating sample magnetometry (Microsense EZ9, USA), respectively. The functional groups of the materials were examined by Fourier-transform infrared spectroscopy (FTIR, Nicolet iS50, Thermo Scientific, USA). Raman spectroscopy (LabRAM HR 800, HORIBA, Japan) was employed to analyze the molecular structure of materials and the interactions between them. Specific surface area and pore size were measured by the Brunauer–Emmett–Teller technique (TriStar 3000, Micromeritics, USA). UV-Visible diffuse reflectance spectroscopy (UV-Vis DRS, JASCO V-770, Japan) was used to determine the absorption wavelength and bandgap energy of the catalyst material. Besides, the point of zero charge (pH_{pzc}) of the material was determined by the titration method. The initial pH value (pH_i) of 11 Erlenmeyer flasks containing 25 mL of 0.01 M NaCl solution was adjusted in the range of 2–12 by adding 0.1 M HCl or NaOH solutions. The solutions were then added with 0.1 g of Fe_3O_4@TiO_2 material, and shaken at 120 rpm for 48 h before filtering. The final pH of the filtrate (pH_f) was then measured and a chart of pH_i vs. ΔpH (i.e., $pH_i - pH_f$) was plotted. The pH_{pzc} of the material is the pH_i where ΔpH = 0.

2.2. Photocatalytic experiments

The photocatalytic experiments were conducted using a lab-scale photocatalytic reactor (Fig. S1) with a volume of 2 L. At first, the synthetic water containing ENR was prepared with a certain ENR concentration (5–25 mg/L). Next, the initial solution pH was adjusted to the desired values (5.5–7.5) by HCl or NaOH solutions. Then, a certain dose of catalyst (0.25–1.25 g/L) was added to the solution. Under UV irradiation (Panasonic FL8BL-B, 8 W, maximum intensity at wavelength of 352 nm), the ENR concentration of the reaction solution was monitored every 30 min. The samples were collected and centrifuged at 6,000 rpm for 15 min. After letting still for 5 min, the solution was filtered to completely remove the materials before ENR concentration measurement. The ENR removal was also verified by an experiment comparing the treatment efficiency of the photolysis, adsorption, and photocatalysis under optimal conditions.

The ENR concentration was analyzed by spectrophotometry using a UV-Vis spectrophotometer (Hitachi U-2910, Japan). The UV absorbance of ENR at concentrations of 5, 10, 15, 20, and 25 mg/L in Fig. S2 shows that the ENR has the highest absorbance at λ = 275 nm, which is similar to the previous studies [28–30]. Therefore, the ENR calibration curve in this study was constructed at the wavelength of 275 nm to determine ENR concentration in the water samples. The degradation efficiency (E, %) is calculated by Eq. (1), where C_o and C_t (mg/L) are the ENR concentrations at the beginning and certain time (t, min), respectively.

$$E = \frac{C_0 - C_t}{C_0} \times 100\% \tag{1}$$

The Langmuir–Hinshelwood (L–H) model is commonly used to investigate the kinetics of heterogeneous catalytic processes [Eqs. (2) and (3)] [31]. The half-life ($t_{1/2}$) is the time required for the pollutant concentration to be reduced by half from the initial concentration, which is determined experimentally or calculated by Eq. (4).

$$\ln\left(\frac{C_0}{C_t}\right) = K_{obs} \times t \tag{2}$$

$$\frac{1}{K_{obs}} = \frac{1}{K_{LH} \times K_C} + \frac{C_0}{K_C} \tag{3}$$

$$t_{1/2} = \frac{\ln 2}{K_{LH} \times K_C} + \frac{C_0}{2 \times K_C} \tag{4}$$

where K_{obs} (mg/L·min) is the first-order degradation rate constant. K_C (mg/L·min) is the surface reaction rate, and K_{L-H} (L/mg) is the Langmuir–Hinshelwood constant.

The Design-Expert software was used to design the experiments and determine the optimal operating conditions of pH value, photocatalyst dosage, and initial concentration for ENR degradation by response surface methodology (RSM). The treatment efficiency was selected as an objective function with the variables of pH, input ENR concentration

(mg/L), catalyst dose (g/L), and treatment time (min). The experiments were designed based on the RSM using the central composite design (CCD) model. The experimental center (point 0) and the survey range (–α, +α) of the parameters were selected based on the previous experimental results. Symbols and values of experimental design parameters are summarized in Table 1 with a total of 30 experiments and each experiment center repeated 6 times. These surveyed experiments were conducted with the same procedure as above, and the ENR degradation efficiency was recorded. The degree of influence of the variables on the objective function is determined through the regression equation by Design-Expert software.

3. Results and discussion

3.1. Characterization of materials

The morphology of the materials observed by SEM is shown in Fig. 1. From these SEM images, material samples are granular, with unequal sizes, especially with Fe_3O_4@TiO_2. Fig. 1c shows that the Fe_3O_4@TiO_2 sample appears locally agglomerated, and the particles adhere to each other to form larger clusters, making the surface of Fe_3O_4@TiO_2 material appear rougher than that of TiO_2 (Fig. 1a). The TiO_2 gel interacts with the Fe_3O_4 particles, forming the core-shell Fe_3O_4@TiO_2 material with a size larger than that of Fe_3O_4 (Fig. 1b).

The EDX-mapping results in Figs. 2 and S3 show the presence of C, O, and Ti elements on the surface of TiO_2, and C, Fe, and O on the surface of Fe_3O_4 materials. The presence of Fe on the surface of Fe_3O_4@TiO_2 material was also observed, proving that not all the surface of Fe_3O_4 was covered by TiO_2. The mass composition of elements on the surface of TiO_2 materials synthesized by the sol–gel method from TTIP precursors with the total content of two elements of O and Ti accounted for 95.35%, showing that TiO_2 was successfully synthesized (Fig. S3a). The remaining 4.65% of C content may be because the precursor TTIP ($C_{12}H_{28}O_4Ti$) was not completely oxidized. The Fe_3O_4 surface had more than 94% of Fe and O elements, and the rest was C (Fig. S3b). For the Fe_3O_4@TiO_2 material, three elements of O, Ti, and Fe (41.775%, 18.63%, and 34.19%, respectively) appeared on the surface with a total ratio of 94.59% (Fig. S3c). With the goal of synthesizing a magnetic photocatalyst with a magnetic core of Fe_3O_4 and photocatalytic shell of TiO_2, the presence of Fe element on the material surface showed that the Fe_3O_4@TiO_2 synthesis process in this study was not optimal. Furthermore, the ratio of Fe element found on the surface was approximately twice that of Ti, suggesting that Fe_3O_4 was not completely covered by TiO_2. This can make the Fe_3O_4@TiO_2 material have a lower photocatalytic efficiency than the TiO_2 material. Therefore, further studies on the material synthesis are needed to improve the catalyst core-shell structure to optimize the photocatalytic and magnetic properties.

Table 1
Surveyed variables and intervals

Independent variables	Symbol	Interval				
		–α	–1	0	+1	+α
pH	x_1	5.5	6	6.5	7	7.5
Enrofloxacin initial concentration	x_2	5	10	15	20	25
Catalyst dosage	x_3	0.25	0.5	0.75	1	1.25
Reaction time	x_4	60	90	120	150	180

The crystalline structure of the materials was determined by XRD (Fig. 3). The XRD patterns clearly display the peaks of anatase at 2θ of 25.24 (101), 37.72 (004), 48.00 (020), 54.98 (121), and 62.62 (204), and there is no rutile peak appeared [24]. In the Fe_3O_4@TiO_2 pattern, in addition to the peaks characteristic of the anatase phase, the peaks at 2θ of 33.2 (104), 35.5 (311), 43.2 (400), and 57 (511) [24] are typical for Fe_3O_4 crystals. The anatase crystalline phase can help the material surface to be easily hydrated to form hydroxyl groups, which creates favorable conditions for O_2 adsorption to promote the fast formation of reactive oxygen species (ROSs). Since the anatase crystalline phase structure still remains after coating TiO_2 gel on Fe_3O_4 ferromagnetic particles, it is expected that Fe_3O_4@TiO_2 materials can still maintain the inherent photocatalytic ability of TiO_2. The XRD and EDX-mapping results show the simultaneous presence of C, O, Ti, and Fe elements in Fe_3O_4@TiO_2 material, which is a positive sign for the high photocatalytic and magnetic ability of the synthesized material.

The magnetic properties of the materials were determined using a vibrating sample magnetometer. The magnetic hysteresis in Fig. 4 shows that the material has quite obvious ferromagnetic characteristics. When increasing the external magnetic field from 0 to 10,000 Oe, the magnetization increased gradually and reached saturation at

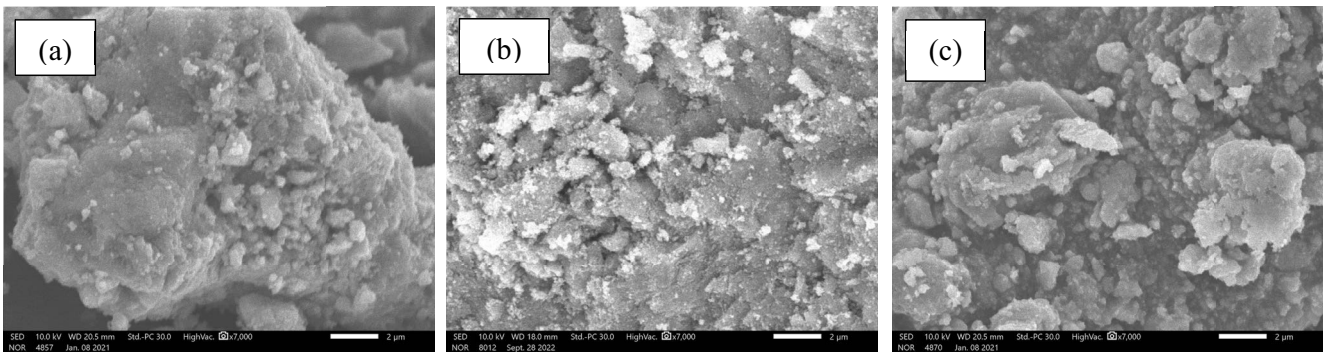

Fig. 1. Scanning electron microscopy images of (a) TiO_2, (b) Fe_3O_4, and (c) Fe_3O_4@TiO_2 materials.

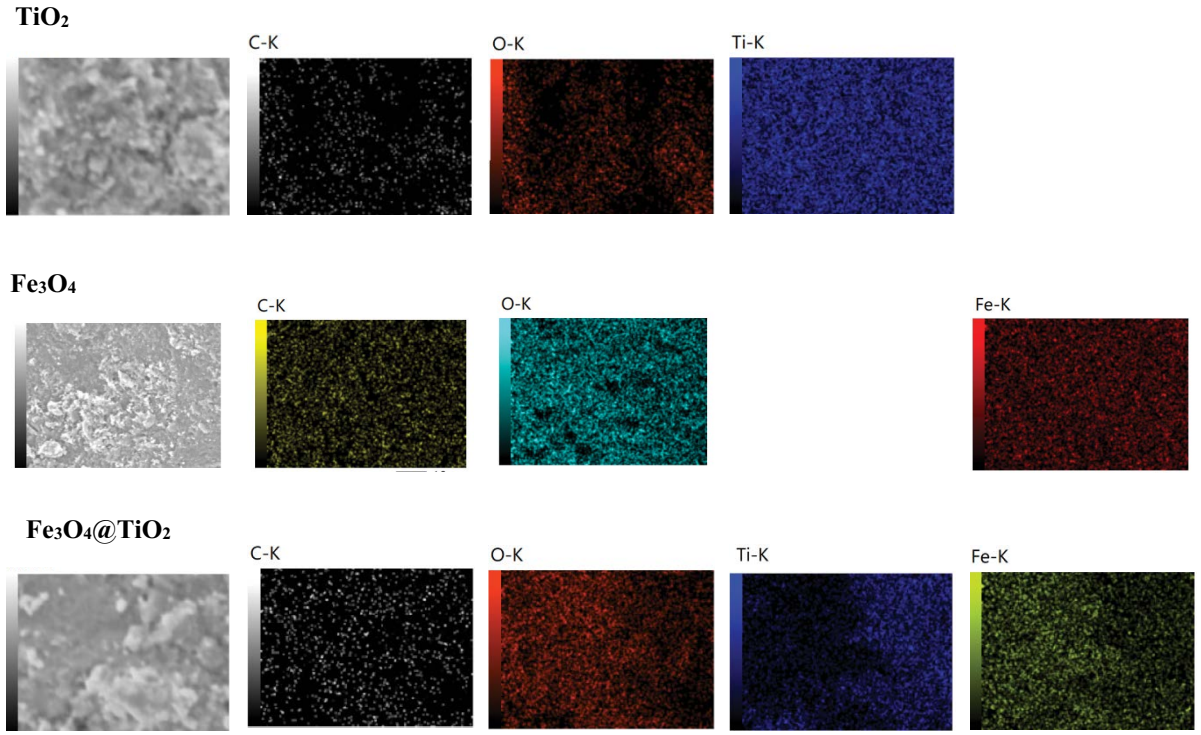

Fig. 2. Energy-dispersive X-ray spectroscopy-mapping results of TiO_2, Fe_3O_4, and Fe_3O_4@TiO_2 materials.

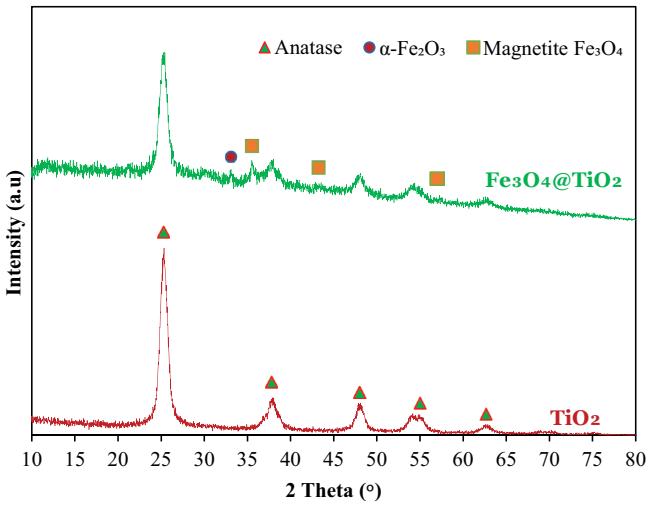

Fig. 3. X-ray diffraction result of TiO_2 and Fe_3O_4@TiO_2 materials.

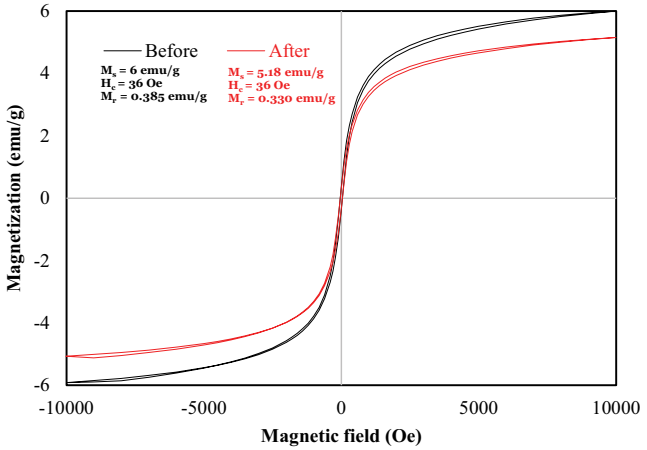

Fig. 4. Magnetic hysteresis loops of Fe_3O_4@TiO_2 material before (black) and after (red) enrofloxacin treatment.

M_s = 6 emu/g. This value is similar to that reported by He et al. [25] (5.94 emu/g) while much smaller than Fe_3O_4-TiO_2 in the study of Noval and Carriazo [24] (49 emu/g). For the material recovered after the photocatalysis, the saturation magnetization was slightly reduced to 5.18 emu/g. The coercive force (H_c) and residual coercivity (M_r) of the two materials before and after ENR treatment are similar, as also noted in Fig. 4. Normally, magnetic materials can be divided into two main categories: "soft" and "hard" magnetic materials with the coercive force of <100 A/m and >100,000 A/m, respectively [32]. The Fe_3O_4@TiO_2 synthesized in this study has a coercive force of ~36 Oe (i.e., 2,865 A/m), thus it is classified as a special semi-hard magnetic material [32]. The relatively small coercive force shows that the material has a weak magnetic dipole moment that cannot overcome the resistance of water. Together with the continuous stirring condition, the material was evenly dispersed during ENR treatment (Fig. S4a). Fig. S4b shows the Fe_3O_4@TiO_2 material with good magnetic recovery, which is promising for practical applications.

The FTIR spectra in the range of 4,000–400 cm^{-1} show that there are similarities between the composite material (Fe_3O_4@TiO_2) and the original materials (TiO_2 and Fe_3O_4) (Fig. 5).

In that, the specific vibration of the Ti–O bond is observed at about 493–728 cm^{-1} [33], which may be the anatase phase [34]. Peaks at 588 and 439 cm^{-1} are assigned to the Fe–O functional group [33,34]. The existence of free water molecules H–O–H and water-adsorbed O–H on the surface of the materials can be seen through peaks at 1,630 and 3,420 or 3,440 cm^{-1}, respectively [34]. Compared to Fe_3O_4, the peaks of the Fe_3O_4@TiO_2 sample were shifted and even disappeared, indicating that TiO_2 was successfully coated on the surface of the Fe_3O_4 material, thereby changing its material characteristics.

Raman spectra of TiO_2, Fe_3O_4, and Fe_3O_4@TiO_2 are exhibited in Fig. 6. The peaks associated with the anatase phase of TiO_2 include 140, 193, 394, 512, and 637 cm^{-1}, corresponding to the segments of E_g, E_g, B_{1g}, A_{1g} + B_{1g}, and E_g [35,36]. The Raman spectrum of Fe_3O_4 has characteristic peaks at 222, 240, 287, 405, 496, 603, 656, and 1,310 cm^{-1} [37]. Among them, the peak at 656 cm^{-1} is identified as the magnetite Fe_3O_4 [37] while the others may be attributed to hematite α-Fe_2O_3 because the exposure to laser light or heat can cause Fe_3O_4 to be oxidized [37,38]. The appearance of characteristic peaks of TiO_2 and Fe_3O_4 in the Raman spectrum of Fe_3O_4@TiO_2 (TiO_2 (at the same position or slightly shifted) showed that Fe_3O_4@TiO_2 composite material was successfully synthesized. However, the weaker peak intensity reveals that the composite material is less magnetic than the original Fe_3O_4 material, which needs to be noticed and improved in further studies.

The specific surface area and pore size of the materials are important parameters to evaluate the activity of a photocatalyst. The N_2 adsorption–desorption results in Fig. 7 show that the Fe_3O_4@TiO_2 material has a hysteresis loop of Type H2(b) according to The International Union of Pure and Applied Chemistry with a strong increase in the adsorption volume from P/P_o ~ 0.7 and steep desorption line, inferring that the material pores are mainly ink-bottle-shaped. Meanwhile, TiO_2 has H3 adsorption–desorption isotherms, corresponding to the wedge-shaped pores. Both TiO_2 and Fe_3O_4@TiO_2 have pore sizes belonging to the mesoporous pore group with relatively large surface areas of 124.5 and 157.5 m^2/g, respectively. This difference indicates a structural change on the surface of the material, where the presence of ferromagnetic Fe_3O_4 particles helps to improve the surface area of the TiO_2 material significantly.

The UV-Vis DRS spectra in Fig. 8 show the difference in absorption edges as well as bandgap (E_g) values of TiO_2 and Fe_3O_4@TiO_2 materials. Specifically, the TiO_2 synthesized from the sol–gel process has a UV-Vis DRS spectrum similar to that of P25 (commercial TiO_2, black line in Fig. 8), with the absorption edge at $\lambda \approx 430$ nm corresponding to an E_g value of 3.10 eV. After combining with ferromagnetic particles, the synthesized Fe_3O_4@TiO_2 material has a red-shift, where the absorption edge shifts to the visible light region with the absorption edge at $\lambda \approx 715$ nm ($E_g \approx 2.65$ eV). This result shows that the synthesized Fe_3O_4@TiO_2 material has a lower activation energy and can work with light sources at longer wavelengths.

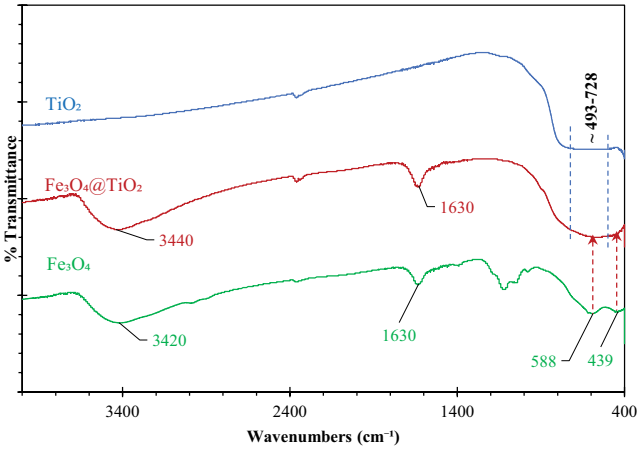

Fig. 5. Fourier-transform infrared spectroscopy spectra of TiO_2, Fe_3O_4, and Fe_3O_4@TiO_2 materials.

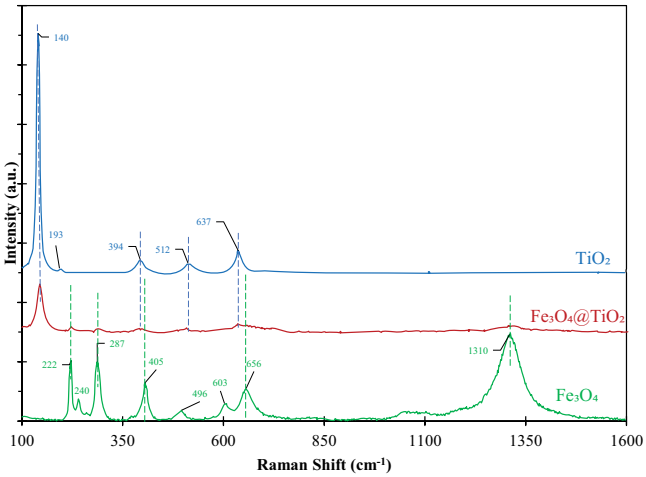

Fig. 6. Raman spectra of TiO_2, Fe_3O_4, and Fe_3O_4@TiO_2 materials.

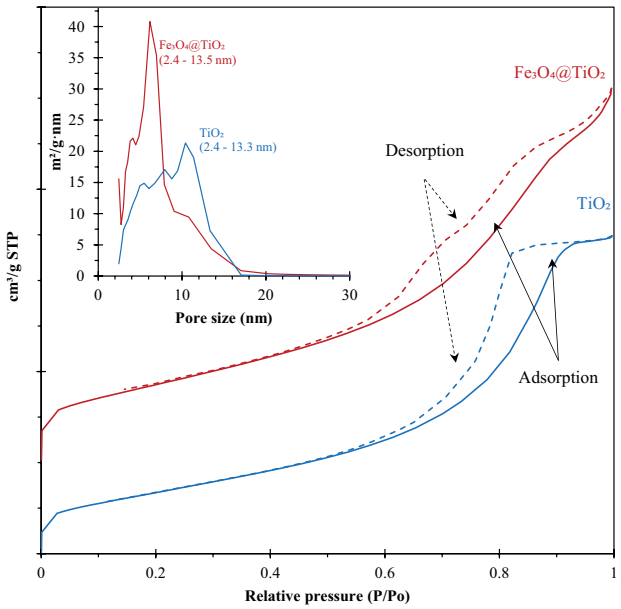

Fig. 7. N_2 adsorption–desorption isotherms of TiO_2 and Fe_3O_4@TiO_2 materials (Inset: pore-size distribution).

3.2. Effects of operating conditions on the ENR degradation

The operating conditions directly affect the performance of the photocatalytic process. The investigation of the change in the pollutant removal efficiency under different conditions forms a basis for the determination of design parameters when deploying the technology on a large scale. Therefore, the effects of pH, catalyst dosage, and initial ENR concentration, as well as retention time on ENR degradation efficiency, were initially investigated.

Fig. 9 displays the change of ENR degradation efficiency at different pH values during 180 min of reaction and the plot for determining the pH_{pzc} of Fe_3O_4@TiO_2. It is observed that the ENR degradation efficiency under neutral and weak alkaline conditions was higher than those under weakly acidic conditions. After 180 min of UV irradiation, ENR removal efficiency was up to 83.78% at pH 7, which is similar to the report of Li et al. [39]. With groups of carboxyl and piperazinyl in the molecular structure, ENR could exist as an anionic, zwitterionic, and cationic species in the aqueous solution depending on the solution pH. This feature can be a great difficulty for determining the interaction mechanism between the pollutant and the catalyst surface since mechanisms such as surface complexation, cation exchange, cation bridging, or electrostatic attraction can simultaneously occur [40].

The surface charge of the material can be estimated through the comparison of its pH_{pzc} with the solution pH. As seen in the inset of Fig. 9, Fe_3O_4@TiO_2 material has a pH_{pzc} value of 6. When solution pH > 6, the surface of the material with a positive charge has the ability to protonate the piperazinyl amine group of ENR, causing ENR cations to be retained at neutral pH [40]. The difference in the degradation efficiency at pH 7 was not very clear from that at pH 7.5. This may be because this pH range lies between the two pK_a values of the ENR (i.e., 6.27 and 8.30), which does not have much effect on the form of ENR in the aqueous solution. However, pH 7 would still be the best choice because aside from the top reason of being the highest ENR degradation efficiency, this value is close to the initial ENR solution pH of 6.45. This would save the amount of chemicals used to adjust the pH of the initial solution.

In the next experiment, the ENR degradation efficiency by photocatalysis was investigated at different catalyst dosages from 0.25 to 1.25 g/L. As shown in Fig. 10, the degradation efficiency increased from 65.89% to 84.65% with an increase in Fe_3O_4@TiO_2 dosage from 0.25 to 1 g/L, which then started to decrease to 83.67% with a further dosage increase to 1.25 g/L. The highest efficiency was reached at the Fe_3O_4@TiO_2 dosage of 1 g/L, which may be because the high concentration of the catalyst (e.g., 1.25 g/L) increases the light scattering, thus hindering the light exposure to the pollutant [41]. Meanwhile, the agglomeration and deposition ability of Fe_3O_4@TiO_2 particles also increase at high concentrations [42,43], thus reducing the degradation efficiency. Finding a suitable catalyst dosage is usually an important step for avoiding excess or insufficient materials for contaminant removal. The photocatalysis using Fe_3O_4@TiO_2 is considered a heterogeneous process, thus the initial reaction rate is proportional to the catalyst concentration. Hence,

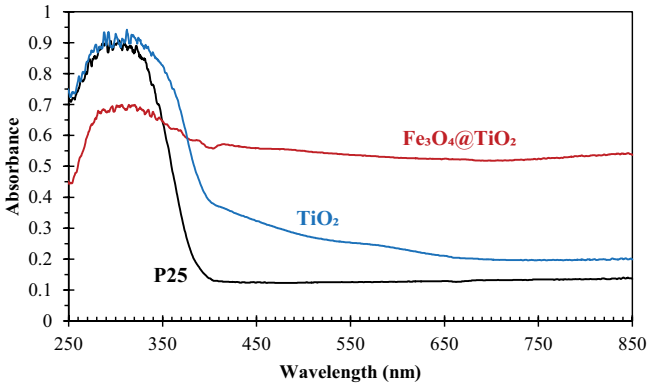

Fig. 8. UV-Visible diffuse reflectance spectra of TiO_2, P25, and Fe_3O_4@TiO_2 materials.

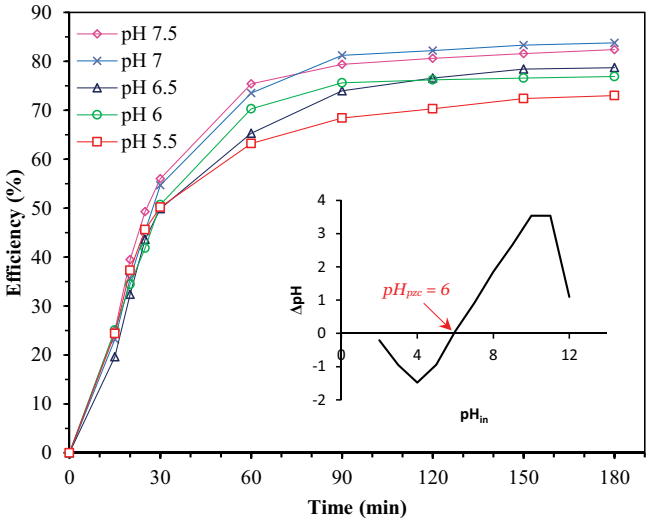

Fig. 9. Effect of initial pH on enrofloxacin degradation efficiency (Inset: plot for determining the pH_{pzc} of Fe_3O_4@TiO_2). (Experimental conditions: [catalyst] = 0.5 g/L, [ENR] = 20 mg/L).

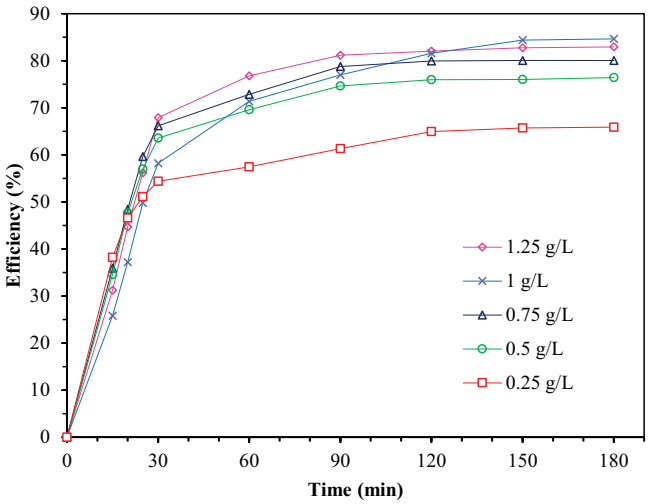

Fig. 10. Effect of catalyst dosage on enrofloxacin degradation efficiency.

after reaching a certain value, the more the catalyst dosage increases, the slower the reaction rate will be, which then no longer depends on the catalyst dosage. The essence of photocatalysis is that a sufficiently large source of photon energy is required. Therefore, with too high catalyst dosage, they could block part of the surface of the material to be illuminated, resulting in a part of the material in the solution is not efficient for photocatalytic reaction.

The initial concentration of the pollutant is one of the important design parameters that directly affect its degradation efficiency. As depicted in Fig. 11, the ENR degradation efficiency after 180 min increased from 77.30% to 92.20% when the initial ENR concentration was decreased from 25 to 10 mg/L. However, when the concentration continued to decrease, the degradation efficiency decreased to only 88.00% at the ENR concentration of 5 mg/L. The ENR degradation rate was consistent with the first-order kinetic model with $R^2 > 0.92$ (Fig. S5), where the highest degradation rate was obtained at the concentration of 10 mg/L with a constant K_{obs} = 0.017 mg/L·min (R^2 = 0.9576) corresponding to the highest degradation efficiency.

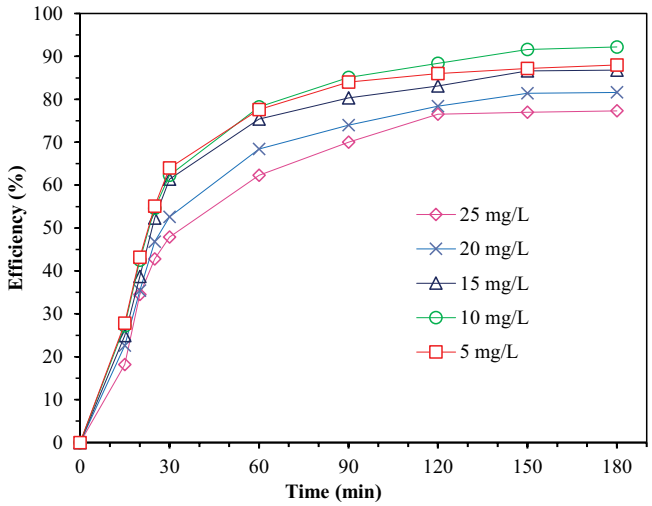

Fig. 11. Effect of the enrofloxacin initial concentration on its degradation efficiency.

The photocatalytic treatment efficiency is directly affected by the interactions of photon-catalyst and pollutant-catalyst and one of the important factors influencing these two interactions is the pollutant concentration. With a moderate pollutant concentration, light can activate the catalyst and the pollutant can also interact well with the catalyst. However, too high pollutant concentration can interfere with the photocatalyst activation since the pollutant molecules attached to the surface of the material can cause the catalyst to be inactive, thus reducing the degradation efficiency. In contrast, the interaction between the pollutant and the catalyst is limited at too low concentrations, and this also reduces the overall degradation efficiency. From the experimental results, it can be concluded that the suitable ENR concentration range for photocatalytic treatment with Fe_3O_4@TiO_2 was from 5 to 20 mg/L with degradation efficiencies of >80%.

The calculated results according to Eqs. (2) and (3) are depicted in Fig. 12a. As the concentration of ENR increases, its photon adsorption also increases, thus significantly losing the number of photons for utilizing by Fe_3O_4@TiO_2 and causing a shortage of photons on the active surface of Fe_3O_4@TiO_2. At the same time, the high ENR concentration could occupy a larger number of active site positions on the surface of Fe_3O_4@TiO_2, which prevents the formation of strong oxidizing radicals, leading to a reduction in the ENR degradation efficiency [39]. The degradation rate varied with each different ENR concentration. However, when evaluating all investigated concentration ranges, the correlation coefficient R^2 of the first-order linear equations was high (i.e., 0.8099), proving the reliability of this equation when applied in practice. Thereby, it can be concluded that the reaction kinetics of ENR follows the Langmuir–Hinshelwood model. The K_C and K_{L-H} values were calculated to be 0.6019 mg/L·min

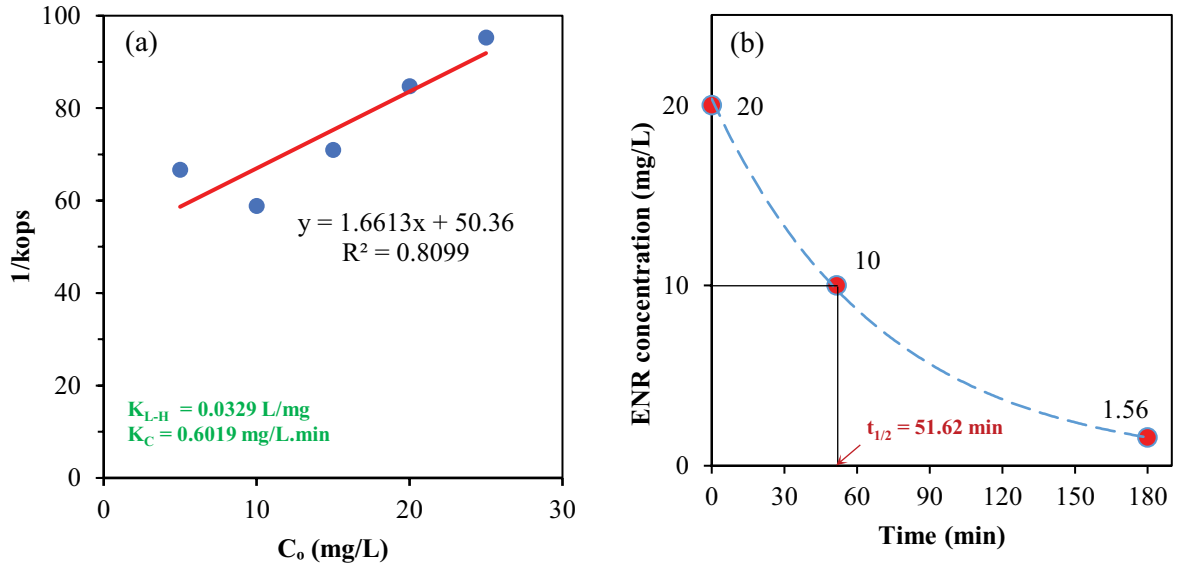

Fig. 12. (a) Kinetics according to Langmuir–Hinshelwood model and (b) the half-life of enrofloxacin at C_o = 20 mg/L.

and 0.0329 L/mg, respectively. Based on the K_C and K_{LH} values, the half-life of the ENR at the initial concentration of 20 mg/L was determined to be 51.62 min (Fig. 12b).

The stability of the ENR degradation process was investigated for 270 min with the best operating conditions found in the above experiments. The ENR degradation efficiency and absorption spectra of the samples in Fig. 13 show that the system operated stably and reached an efficiency of 93.70% after 270 min. According to the reaction time, the ENR degradation efficiency increased gradually in three stages: (i) rapid increase for the first 30 min, (ii) slow increase for the next 150 min, and (iii) reaching equilibrium for the rest time. In the starting stage of the reaction, the ENR density is high, and the uncovered surface area of the catalyst is large, which helps the degradation take place quickly. Moreover, high ENR concentrations can promote the shift of the equilibrium toward the direction of decreasing ENR concentration. Over time, the free surface area of the catalyst decreases, and the ENR density also decreases, thus the degradation rate is reduced and the degradation efficiency increases slowly. In the last state, without the addition of both ENR and Fe_3O_4@TiO_2, the process gradually reaches equilibrium. Therefore, the degradation efficiency in this period was almost unchanged. The results of the absorption spectra of the samples after treatment showed similar peaks at the wavelength range from 200 to 400 nm with the peak intensity decreasing during the reaction time (inset of Fig. 9). The peak with the highest intensity of all samples was obtained at 275 nm, which was not changed during the reaction time. This important experimental data suggests that the ENR degradation took place completely and yielded no other products/intermediates. This is an important result for the development of photocatalytic degradation of antibiotics using Fe_3O_4@TiO_2 material in the future.

3.3. Optimization of ENR degradation

The results of the analysis of variance in Table 2 show that there is a statistically significant difference between the variables (i.e., *P*-values < 0.05). The coefficient of determination R^2 is the ratio of the variable to be interpreted as the mean sum of the variables and a measure of model fit. When R^2 is close to 1, it means that the experimental value of the experimental model is more consistent with reality. Although the R^2 value of 0.84 in this work is not high, it is sufficient to confirm that the empirical polynomial model built in this test is consistent with the actual situation.

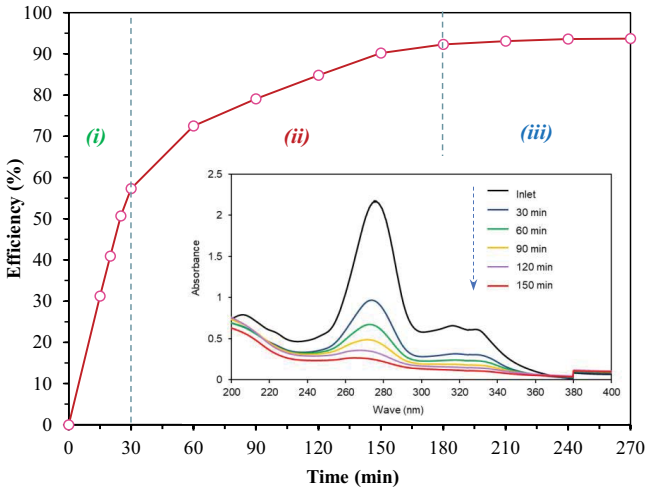

Fig. 13. Enrofloxacin degradation efficiency over time (Inset: absorption spectra of enrofloxacin samples during the reaction time).

The influence of the investigated variables on the degradation efficiency was expressed through the objective function with pH (x_1), ENR initial concentration (x_2), catalyst dosage (x_3), and reaction time (x_4). As presented in Table 3 and Fig. 14, the empirical quadratic polynomial is expressed in Eq. (5) with the omitted variables that are not significant (*P*-value > 0.05).

$$Y = 80.61 + 5.24x_1 - 4.92x_2 + 3.73x_3 + 2.37x_4 + 5.23x_1x_2 + 3.581x_1x_3 \quad (5)$$

The optimal conditions found for this model were at a catalyst dosage of 0.972 g/L, initial ENR concentration of 19.628 mg/L, pH 7, and reaction time of about 149.85 min. After conducting 6 iterations of the experiment based on the optimal parameters for the model, the degradation efficiency was from 91% to 95%, and the possibility of error due to noise was within the allowable range (<5%). This result confirms again the high efficiency of ENR degradation by photocatalysis using Fe_3O_4@TiO_2 material as well as the appropriateness of the model in practical applications.

3.4. Fe_3O_4@TiO_2 recovery and reuse testing

The reusability of Fe_3O_4@TiO_2 materials is a matter of particular interest in this study. The material recovery and reuse experiment were conducted with the optimal conditions found such as catalyst dosage of 0.972 g/L, initial ENR concentration of 19.628 mg/L, and pH 7. The results in Fig. 15 show that the ENR degradation efficiency achieved at the reuse of the material was lower than that of the first time. In the first stage (0–30 min) the difference was not significant, but later on, the material used for the first time gave a much better degradation efficiency. Specifically, at 180 min, this difference was about 1.3 times. This may be because the material structure cannot be maintained in the same condition after being used, thus causing a decrease in the photocatalytic degradation efficiency.

Table 2
Results of analysis of variance for the multivariable quadratic model

Source	Sum of squares	df	Mean squares	*F*-values	*P*-values
Model	2,349.43	6	391.57	20.23	<0.0001
Residual	445.08	23	19.35	–	–
Lack of fit	444.92	18	24.72	745.41	<0.0001
Pure error	0.1658	5	0.0332	–	–
Total	2,794.52	29	–	–	–
R^2 = 0.8407					

Table 3
Coefficient of the regression equation and *P*-values

Factor	Coefficient estimate	df	Standard error	95% CI low	95% CI high	*F*-value	*P*-value
Intercept	80.61	1	0.8686	78.80	82.43	–	–
x_1	5.24	1	0.9712	3.21	7.27	29.09	<0.0001
x_2	–4.92	1	0.9712	–6.95	–2.88	25.63	<0.0001
x_3	3.73	1	0.9712	1.70	5.76	14.4	0.0004
x_4	2.37	1	0.9712	0.3373	4.40	5.96	0.0147
x_1x_2	5.23	1	1.19	2.74	7.72	19.33	<0.0001
x_1x_3	3.58	1	1.19	1.09	6.06	9.03	0.0035
x_1x_4	0.4325	1	1.19	–2.06	2.92	0.1322	0.7202
x_2x_3	–0.0200	1	1.19	–2.51	2.47	0.0003	0.9868
x_2x_4	–0.0375	1	1.19	–2.53	2.45	0.001	0.9752
x_3x_4	–0.8650	1	1.19	–3.35	1.62	0.5289	0.4760

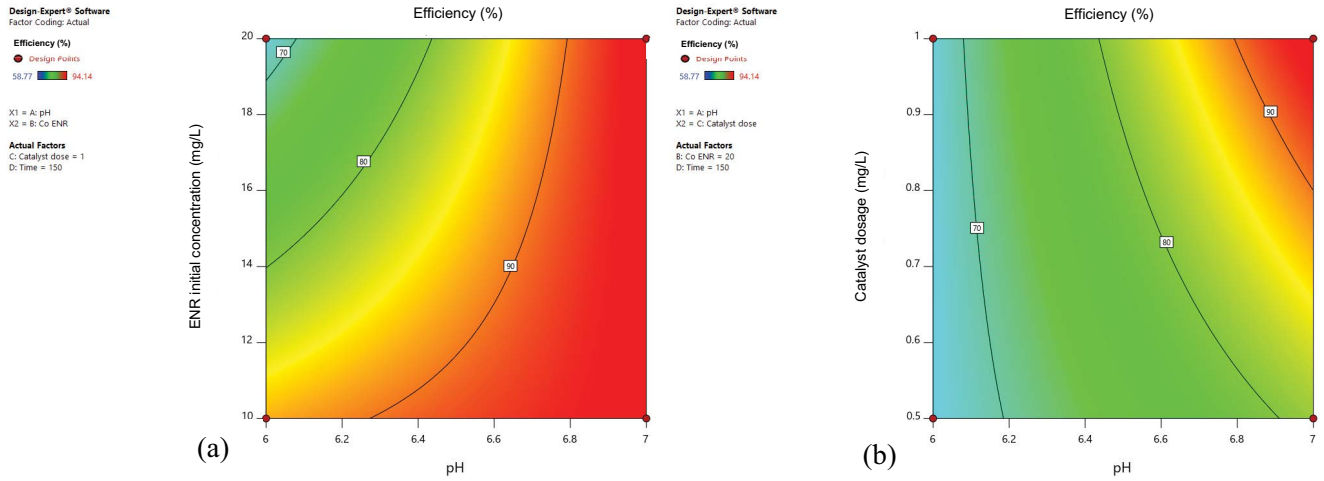

Fig. 14. Response surface graph of survey elements: (a) pH and enrofloxacin initial concentration and (b) pH and catalyst dosage.

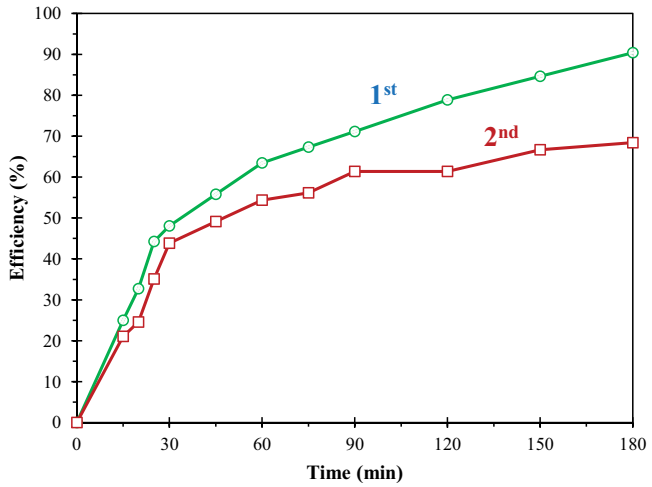

Fig. 15. Fe_3O_4@TiO_2 recovery and reuse testing. (Experimental conditions: [catalyst] = 0.972 g/L, [ENR] = 19.628 mg/L, pH 7).

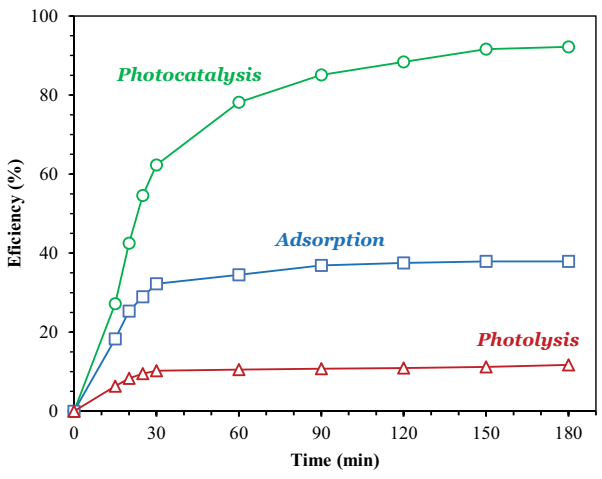

Fig. 16. Enrofloxacin degradation efficiency by photolysis, adsorption, and photocatalysis.

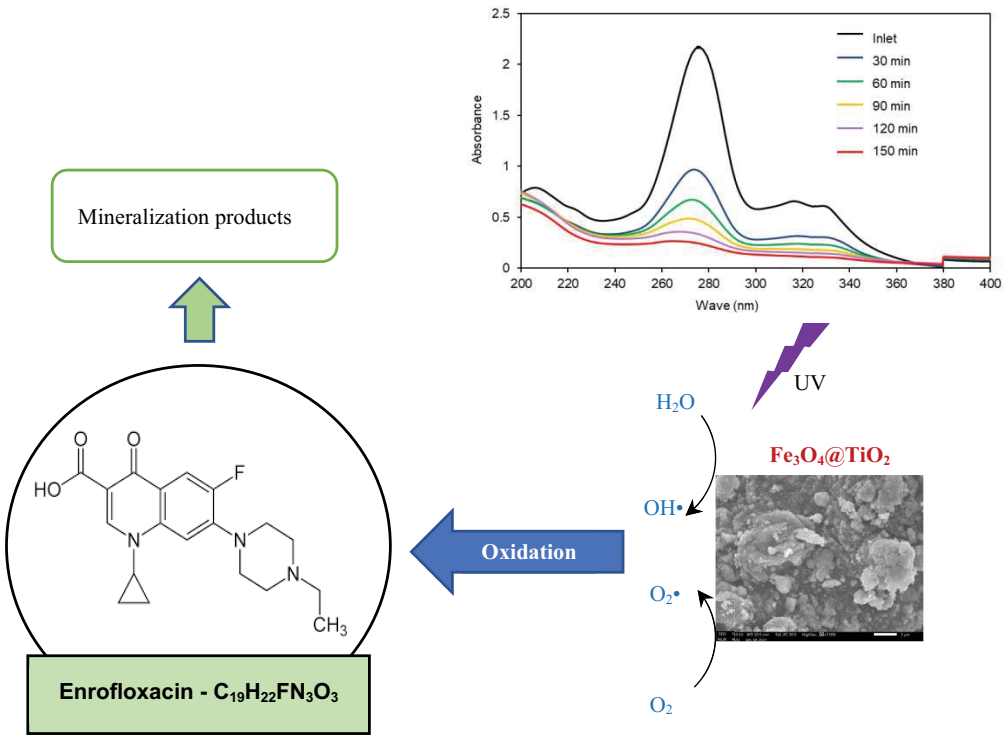

Fig. 17. Mechanism of enrofloxacin degradation by Fe_3O_4@TiO_2 under UV light.

3.5. Mechanism and limitation of this study

To evaluate the ENR degradation ability by various methods using Fe_3O_4@TiO_2, photolysis, adsorption, and photocatalysis tests were conducted. The values of catalyst dosage, pH, initial ENR concentration, and reaction time were established under optimal conditions and the experimental results are shown in Fig. 16. Apparently, only about 11.72% of ENR was photolyzed by UV after 180 min and 37.9% of ENR was adsorbed by Fe_3O_4@TiO_2 after about 60 min, which started to reach the equilibrium. However, more than 92.2% of ENR was degraded in photocatalysis. In addition, the same experiment was carried out with no light on for the first 30 min (Fig. S6). These obtained results were similar to when in dark conditions, where the efficiency achieved was much lower than that of UV irradiation, indicating the synergistic effect between material and UV light [44]. A study by Yu et al. [26] also evaluated the ENR degradation ability over time under sunlight conditions and the adsorption by Fe_3O_4@TiO_2 gave similar results to this experimental result. Over time, ENR concentrations tended to decrease in all 3 methods (Fig. 16). However, with the same concentration, the photocatalysis using Fe_3O_4@TiO_2 material gave the highest degradation and almost completely eliminated the ENR after only 150 min of UVA irradiation. This is an important conclusion in evaluating the treatment efficiency as well as the applicability of this option in the actual treatment of ENR.

Based on the literature review and our own experiences, the mechanism of ENR degradation in this study is proposed in Fig. 17. Accordingly, when being stimulated by UV light, the Fe_3O_4@TiO_2 catalyst helps the ENR degradation process to take place faster with the main role of ROSs such as $OH^•$ and $O_2^{•-}$. These two ROSs could break ENR down into simpler or mineralized products that are less harmful to the environment. In-depth investigations with intensive experiments (e.g., radical scavenging test, ion effects, electron paramagnetic resonance spectroscopy test, determination of intermediates (by mass spectroscopy) and mineralized products (by ion chromatography) [45,46]) are necessary for future works to give a comprehensive photocatalytic mechanism of UV-irradiated Fe_3O_4@TiO_2 and ENR degradation pathway.

4. Conclusion

The Fe_3O_4@TiO_2 materials were initially successfully synthesized with the expected ENR degradation efficiency of over 90%. The optimal condition obtained from an experimental design by Design-Experts was at a catalyst dosage of 0.972 g/L, initial ENR concentration of 19.628 mg/L, and pH 7. Experiments show that the main mechanism of degradation is photocatalysis, although the initial stage depends heavily on adsorption on the surface. The ability to recover and reuse materials shows many potential practical applications. However, further research and improvement are needed so that the material can maintain its effectiveness after many times of reuse.

Acknowledgement

This research was conducted under the framework of CARE-RESCIF initiative and financially supported by Ho Chi Minh City University of Technology (HCMUT), VNU-HCM

under grant number Tc-MTTN-2021-04. We acknowledge the support of time and facilities from Ho Chi Minh City University of Technology (HCMUT), VNU-HCM for this study.

References

[1] I. Michael, L. Rizzo, C. McArdell, C. Manaia, C. Merlin, T. Schwartz, C. Dagot, D. Fatta-Kassinos, Urban wastewater treatment plants as hotspots for the release of antibiotics in the environment: a review, Water Res., 47 (2013) 957–995.

[2] W.C. Li, Occurrence, sources, and fate of pharmaceuticals in aquatic environment and soil, Environ. Pollut., 187 (2014) 193–201.

[3] K. Kümmerer, Antibiotics in the aquatic environment – a review – Part I, Chemosphere, 75 (2009) 417–434.

[4] P. Gao, M. Munir, I. Xagoraraki, Correlation of tetracycline and sulfonamide antibiotics with corresponding resistance genes and resistant bacteria in a conventional municipal wastewater treatment plant, Sci. Total Environ., 421 (2012) 173–183.

[5] M.A. Mitchell, Enrofloxacin, J. Exot. Pet. Med., 15 (2006) 66–69.

[6] M. Andrieu, A. Rico, T.M. Phu, D.T.T. Huong, N.T. Phuong, P.J. Van den Brink, Ecological risk assessment of the antibiotic enrofloxacin applied to Pangasius catfish farms in the Mekong Delta, Vietnam, Chemosphere, 119 (2015) 407–414.

[7] J. Gibs, H.A. Heckathorn, M.T. Meyer, F.R. Klapinski, M. Alebus, R.L. Lippincott, Occurrence and partitioning of antibiotic compounds found in the water column and bottom sediments from a stream receiving two wastewater treatment plant effluents in Northern New Jersey, 2008, Sci. Total Environ., 458 (2013) 107–116.

[8] A. Watkinson, E. Murby, D.W. Kolpin, S. Costanzo, The occurrence of antibiotics in an urban watershed: from wastewater to drinking water, Sci. Total Environ., 407 (2009) 2711–2723.

[9] Y. Li, R. Jindal, K. Choi, Y.L. Kho, P.G. de Bullen, Pharmaceutical residues in wastewater treatment plants and surface waters in Bangkok, J. Hazard. Toxic Radioact. Waste, 16 (2012) 88–91.

[10] J. Fick, H. Söderström, R.H. Lindberg, C. Phan, M. Tysklind, D.J. Larsson, Contamination of surface, ground, and drinking water from pharmaceutical production, Environ. Toxicol. Chem., 28 (2009) 2522–2527.

[11] D.G.J. Larsson, C. de Pedro, N. Paxeus, Effluent from drug manufactures contains extremely high levels of pharmaceuticals, J. Hazard. Mater., 148 (2007) 751–755.

[12] R. Wei, F. Ge, M. Chen, R. Wang, Occurrence of ciprofloxacin, enrofloxacin, and florfenicol in animal wastewater and water resources, J. Environ. Qual., 41 (2012) 1481–1486.

[13] M. Sturini, A. Speltini, F. Maraschi, A. Profumo, L. Pretali, E.A. Irastorza, E. Fasani, A. Albini, Photolytic and photocatalytic degradation of fluoroquinolones in untreated river water under natural sunlight, Appl. Catal., B, 119 (2012) 32–39.

[14] W. Yan, J. Zhang, C. Jing, Enrofloxacin transformation on *Shewanella oneidensis* MR-1 reduced goethite during anaerobic–aerobic transition, Environ. Sci. Technol., 50 (2016) 11034–11040.

[15] X.-x. Zhang, Y.-g. Xiao, S.-s. Cao, Z.-l. Yin, Z.-Q. Liu, Ternary TiO_2@Bi_2O_3@TiO_2 hollow photocatalyst drives robust visible-light photocatalytic performance and excellent recyclability, J. Cleaner Prod., 352 (2022) 131560, doi: 10.1016/j.jclepro.2022.131560.

[16] A.L. Giraldo, G.A. Penuela, R.A. Torres-Palma, N.J. Pino, R.A. Palominos, H.D. Mansilla, Degradation of the antibiotic oxolinic acid by photocatalysis with TiO_2 in suspension, Water Res., 44 (2010) 5158–5167.

[17] X. Hu, X. Hu, Q. Peng, L. Zhou, X. Tan, L. Jiang, C. Tang, H. Wang, S. Liu, Y. Wang, Mechanisms underlying the photocatalytic degradation pathway of ciprofloxacin with heterogeneous TiO_2, Chem. Eng. J., 380 (2020) 122366, doi: 10.1016/j.cej.2019.122366.

[18] N.T.C. Tien, C.H. Nhut, V.T.T. Thuy, T.T.B. Huyen, L.P.T. Hien, N.N. Huy, Enhancement in photocatalytic efficiency of commercial TiO_2 nanoparticles by calcination: a case of doxycycline removal, Bull. Chem. React. Eng. Catal., 17 (2022) 486–496.

[19] X. Chen S.S. Mao, Titanium dioxide nanomaterials: synthesis, properties, modifications, and applications, Chem. Rev., 107 (2007) 2891–2959.

[20] M. Ye, Q. Zhang, Y. Hu, J. Ge, Z. Lu, L. He, Z. Chen, Y. Yin, Magnetically recoverable core–shell nanocomposites with enhanced photocatalytic activity, Chem. Eur. J., 16 (2010) 6243–6250.

[21] A.A. Babaei, M. Golshan, B. Kakavandi, A heterogeneous photocatalytic sulfate radical-based oxidation process for efficient degradation of 4-chlorophenol using TiO_2 anchored on Fe oxides@carbon, Process Saf. Environ. Prot., 149 (2021) 35–47.

[22] S. Moradi, S.A. Sobhgol, F. Hayati, A.A. Isari, B. Kakavandi, P. Bashardoust, B. Anvaripour, Performance and reaction mechanism of MgO/ZnO/graphene ternary nanocomposite in coupling with LED and ultrasound waves for the degradation of sulfamethoxazole and pharmaceutical wastewater, Sep. Purif. Technol., 251 (2020) 117373, doi: 10.1016/j.seppur.2020.117373.

[23] O.F.S. Khasawneh, P. Palaniandy, Removal of organic pollutants from water by Fe_2O_3/TiO_2 based photocatalytic degradation: a review, Environ. Technol. Innovation, 21 (2021) 101230, doi: 10.1016/j.eti.2020.101230.

[24] V.E. Noval, J.G. Carriazo, Fe_3O_4-TiO_2 and Fe_3O_4-SiO_2 core-shell powders synthesized from industrially processed magnetite (Fe_3O_4) microparticles, Mater. Res., 22 (2019) e20180660, doi: 10.1590/1980-5373-MR-2018-0660.

[25] Q. He, Z. Zhang, J. Xiong, Y. Xiong, H. Xiao, A novel biomaterial—Fe_3O_4: TiO_2 core-shell nano particle with magnetic performance and high visible light photocatalytic activity, Opt. Mater., 31 (2008) 380–384.

[26] Y. Yu, L. Yan, J. Cheng, C. Jing, Mechanistic insights into TiO_2 thickness in Fe_3O_4@TiO_2-GO composites for enrofloxacin photodegradation, Chem. Eng. J., 325 (2017) 647–654.

[27] D.H. Dau, L.V. Ngoan, L.M. Tung, T.H. Hai, Synthesizing super paramagnetic nanoparticle Fe_3O_4 and crusting procedure, Can Tho Univ. J. Sci., 19a (2011) 38–46.

[28] L.-l. Pei, W.-z. Yang, J.-y. Fu, M.-x. Liu, T.-t. Zhang, D.-b. Li, R.-y. Huang, L. Zhang, G.-n. Peng, G. Shu, Synthesis, characterization, and pharmacodynamics study of enrofloxacin mesylate, Drug Des. Dev. Ther., 14 (2020) 715–730.

[29] H.-t. Zhang, J.-q. Jiang, Z.-l. Wang, X.-y. Chang, X.-y. Liu, S.-h. Wang, K. Zhao, J.-s. Chen, Development of an indirect competitive ELISA for simultaneous detection of enrofloxacin and ciprofloxacin, J. Zhejiang Univ. Sci. B, 12 (2011) 884–891.

[30] P. Huang, J. Luan, Structure and photocatalytic performance of rice husk-like Ba-doped GaOOH under light irradiation, RSC Adv., 9 (2019) 19930–19939.

[31] M. Malakootian, A. Nasiri, M. Amiri Gharaghani, Photocatalytic degradation of ciprofloxacin antibiotic by TiO_2 nanoparticles immobilized on a glass plate, Chem. Eng. Commun., 207 (2020) 56–72.

[32] S. Tumanski, Handbook of Magnetic Measurements, CRC Press, Boca Raton, Florida, 2011.

[33] N.V. Chukanov, A.D. Chervonnyi, Infrared Spectroscopy of Minerals and Related Compounds, Springer International Publishing, Cham, 2016, pp. 1–49.

[34] S. Salamat, H. Younesi, N. Bahramifar, Synthesis of magnetic core–shell Fe_3O_4@TiO_2 nanoparticles from electric arc furnace dust for photocatalytic degradation of steel mill wastewater, RSC Adv., 7 (2017) 19391–19405.

[35] S. Mamedov, Characterization of TiO_2 nanopowders by Raman spectroscopy, Raman Technol. Today's Spectroscopists, 35 (2020) 41–49.

[36] S.S. Al-Taweel, H.R. Saud, New route for synthesis of pure anatase TiO_2 nanoparticles via utrasound-assisted sol–gel method, J. Chem. Pharm. Res., 8 (2016) 620–626.

[37] P. Kumar, H. No-Lee, R. Kumar, Synthesis of phase pure iron oxide polymorphs thin films and their enhanced magnetic properties, J. Mater. Sci.: Mater. Electron., 25 (2014) 4553–4561.

[38] C.P. Bergmann, P.C. Panta, Raman spectroscopy of iron oxide of nanoparticles (Fe_3O_4), J. Mater. Sci. Eng., 5 (2015) 146, doi: 10.4172/2169-0022.1000217.
[39] W. Li, C. Guo, B. Su, J. Xu, Photodegradation of four fluoroquinolone compounds by titanium dioxide under simulated solar light irradiation, J. Chem. Technol. Biotechnol., 87 (2012) 643–650.
[40] W. Yan, S. Hu, C. Jing, Enrofloxacin sorption on smectite clays: effects of pH, cations, and humic acid, J. Colloid Interface Sci., 372 (2012) 141–147.
[41] S. Kansal, M. Singh, D. Sud, Studies on photodegradation of two commercial dyes in aqueous phase using different photocatalysts, J. Hazard. Mater., 141 (2007) 581–590.
[42] N. San, M. Kılıç, Z. Tuiebakhova, Z. Çınar, Enhancement and modeling of the photocatalytic degradation of benzoic acid, J. Adv. Oxid. Technol., 10 (2007) 43–50.
[43] C.M. So, M.Y. Cheng, J.C. Yu, P.K. Wong, Degradation of azo dye Procion Red MX-5B by photocatalytic oxidation, Chemosphere, 46 (2002) 905–912.
[44] S. Moradi, A.A. Isari, F. Hayati, R. Rezaei Kalantary, B. Kakavandi, Co-implanting of TiO_2 and liquid-phase-delaminated g-C_3N_4 on multi-functional graphene nanobridges for enhancing photocatalytic degradation of acetaminophen, Chem. Eng. J., 414 (2021) 128618, doi: 10.1016/j.cej.2021.128618.
[45] Y. Xue, P. Wang, C. Wang, Y. Ao, Efficient degradation of atrazine by BiOBr/UiO-66 composite photocatalyst under visible light irradiation: environmental factors, mechanisms and degradation pathways, Chemosphere, 203 (2018) 497–505.
[46] C. Wang, Y. Xue, P. Wang, Y. Ao, Effects of water environmental factors on the photocatalytic degradation of sulfamethoxazole by AgI/UiO-66 composite under visible light irradiation, J. Alloys Compd., 748 (2018) 314–322.

Supporting information

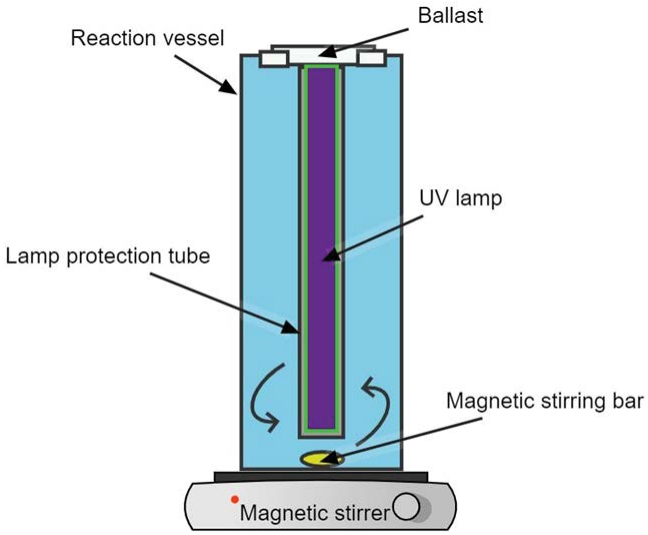

Fig. S1. Lab-scale of photocatalytic reaction model.

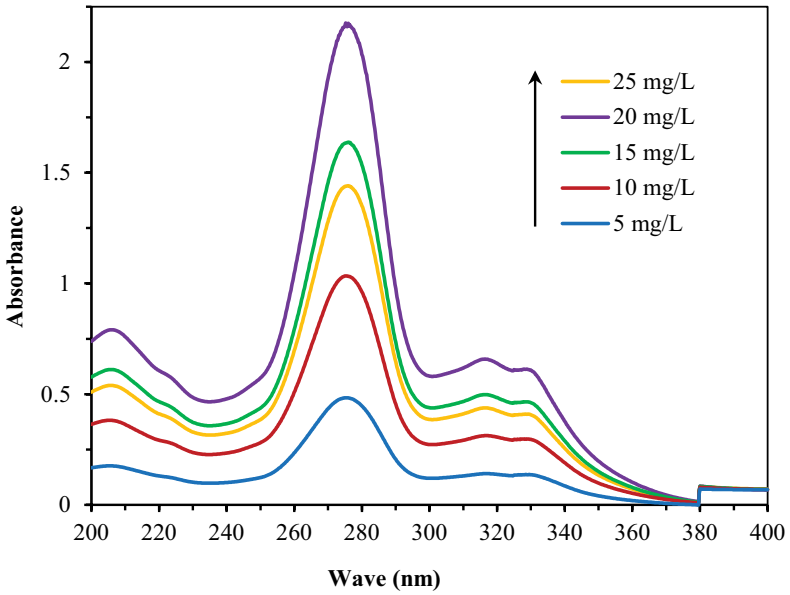

Fig. S2. UV absorbance of enrofloxacin at concentrations in the range of 5–25 mg/L.

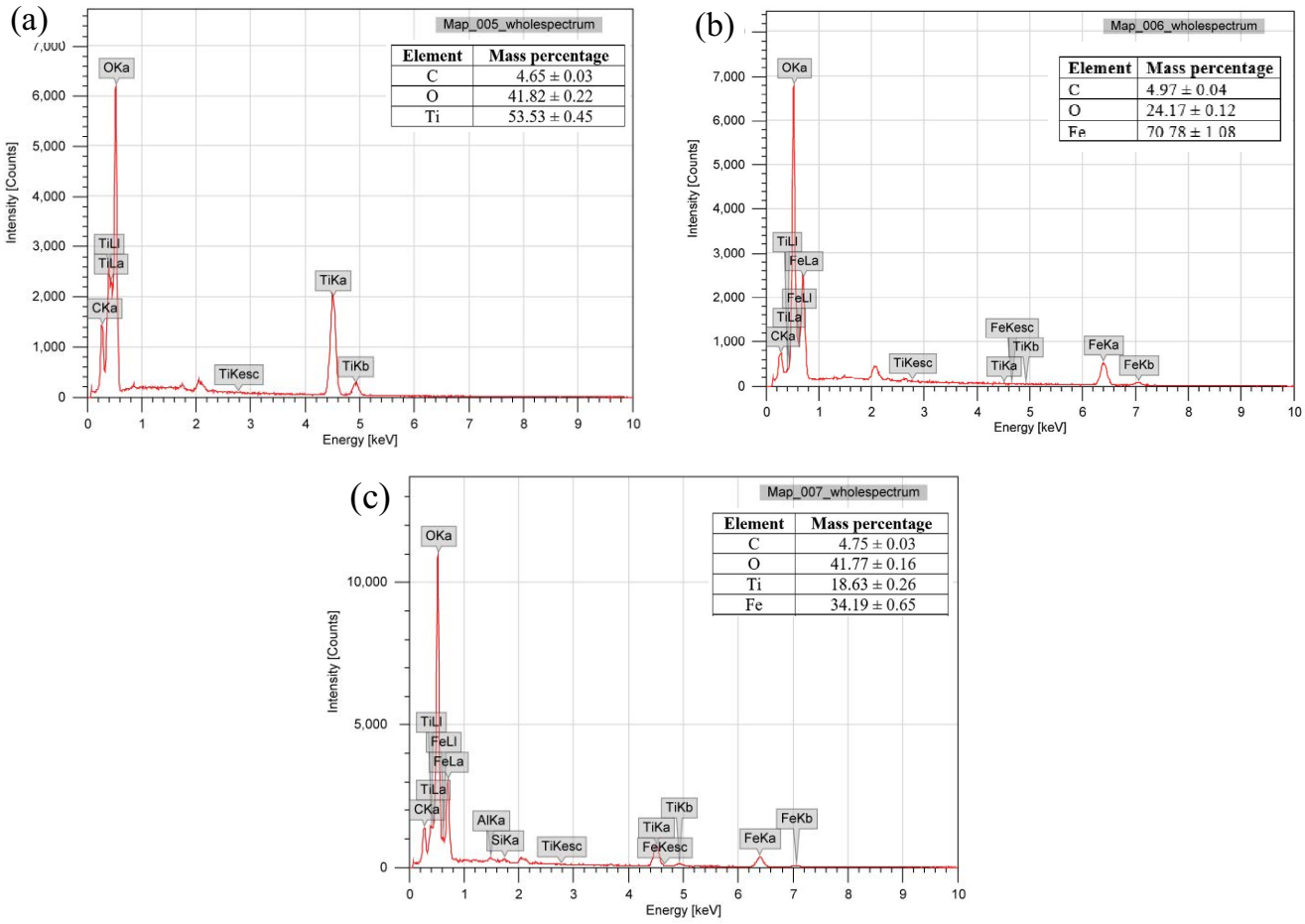

Fig. S3. Energy-dispersive X-ray spectroscopy results of (a) TiO_2, (b) Fe_3O_4, and (c) Fe_3O_4@TiO_2.

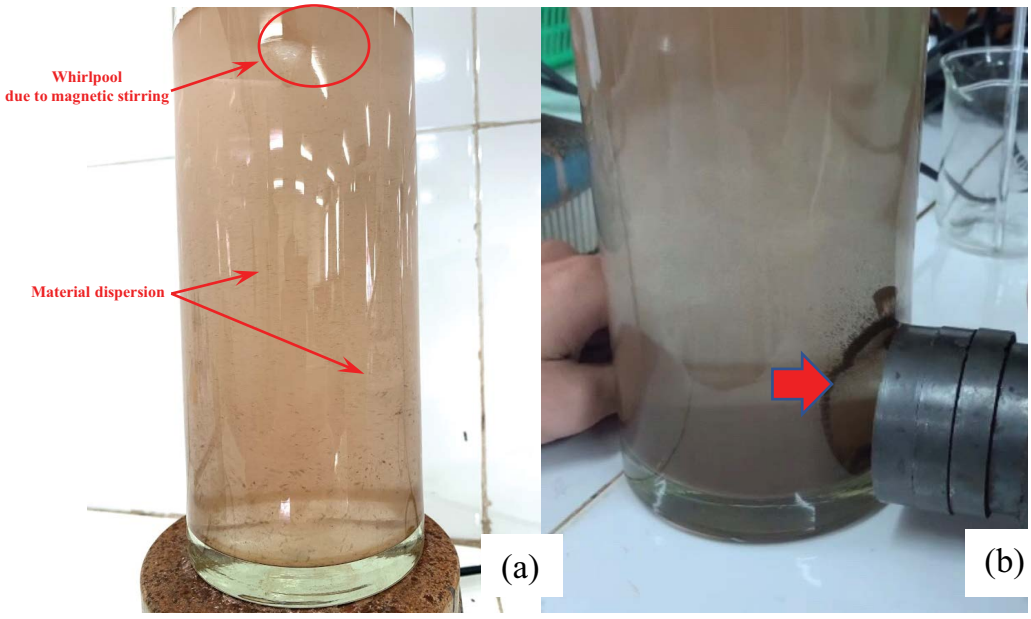

Fig. S4. (a) Material dispersion during processing and (b) material recovery.

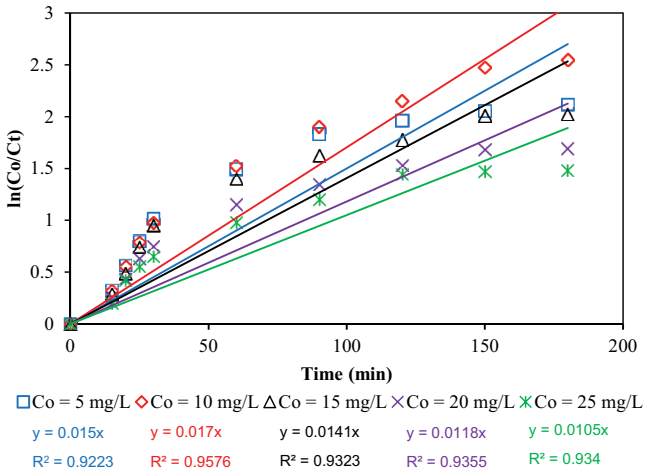

Fig. S5. Degradation rate of enrofloxacin over time.

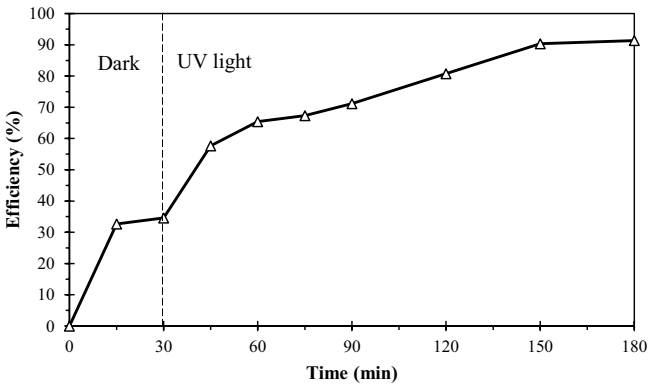

Fig. S6. Adsorption (dark) and photocatalytic degradation (UV light) of enrofloxacin over time.